The Effects of Aircraft Wake Dynamics on Contrail Development

D. C. LEWELLEN AND W. S. LEWELLEN

Department of Mechanical and Aerospace Engineering, West Virginia University, Morgantown, West Virginia

(Manuscript received 17 December 1999, in final form 8 May 2000)

ABSTRACT

Results of large-eddy simulations of the development of young persistent ice contrails are presented, concentrating on the interactions between the aircraft wake dynamics and the ice cloud evolution over ages from a few seconds to ~30 min. The 3D unsteady evolution of the dispersing engine exhausts, trailing vortex pair interaction and breakup, and subsequent Brunt–Väisälä oscillations of the older wake plume are modeled in detail in high-resolution simulations, coupled with a bulk microphysics model for the contrail ice development. The simulations confirm that the early wake dynamics can have a strong influence on the properties of persistent contrails even at late times. The vortex dynamics are the primary determinant of the vertical extent of the contrail (until precipitation becomes significant); and this together with the local wind shear largely determines the horizontal extent. The ice density, ice crystal number density, and a conserved exhaust tracer all develop and disperse in different fashions from each other. The total ice crystal number can be significantly reduced due to adiabatic compression resulting from the downward motion of the vortex system, even for ambient conditions that are substantially supersaturated with respect to ice. The fraction of the initial ice crystals surviving, their spatial distribution, and the ice mass distribution are all sensitive to the aircraft type, ambient humidity, assumed initial ice crystal number, and ambient turbulence conditions. There is a significant range of conditions for which a smaller transport such as a B737 produces as significant a persistent contrail as a larger transport such as a B747, even though the latter consumes almost five times as much fuel. The difficulties involved in trying to minimize persistent contrail production are discussed.

1. Introduction

Aircraft contrails have become a common cloud form, often representing the only visual perturbation in an otherwise cloudless region of sky. What is less readily apparent to the casual observer is that under some conditions contrails can grow, spread, and form what appears from the ground to be naturally occurring cirrus sheets representing significant cloud cover (e.g., Minnis et al. (1998). Given the increase in air traffic projected for the next few decades, the question arises whether contrails may in the future (or even now) perturb the earth's radiation balance through this increased cloud cover. In recent years this issue, along with other potential atmospheric effects of aviation, has stimulated much research (see, e.g., Penner et al. 1999). Many effects have an impact on this problem—the aircraft emissions, chemistry, and contrail formation in the rapidly diluting early exhaust plumes; effects of the aircraft downwash; ice microphysics and radiative properties; the state of the atmosphere within the flight corridors; atmospheric dispersion rates; etc.—and are being actively researched. As part of this larger effort, we focus in this paper on one aspect of contrail development: whether the aircraft wake dynamics occurring from a few seconds to tens of minutes behind the aircraft can have any lasting effects on the resulting contrails.

In the evolution of an aircraft contrail, it is convenient to identify four overlapping regimes. During the first few seconds, the engine exhaust jets rapidly mix with ambient air and, for suitable atmospheric conditions, become supersaturated with respect to water and form a contrail (see, e.g., Schumann 1996). During the same period, the vorticity distribution shed from the wing rolls up into a pair of trailing vortices. The wake dynamics following this roll-up/jet regime are dominated by the interactions of the vortex pair. Typically in this stage the engine exhaust jets partly wrap into the vortex cores and partly detrain into a buoyant plume; the vortices fall and interact with each other through a mutual induction sinusoidal instability (Crow 1970) and with any ambient shear that is present, until they finally break up, typically within a few minutes. Given ambient conditions supersaturated with respect to ice, the contrail can grow as moist air mixes with the ice crystal rich exhaust plume. After vortex breakup, positive buoyancy

Corresponding author address: Dr. David C. Lewellen, Department of Mechanical and Aerospace Engineering, West Virginia University, P.O. Box 6106, Morgantown, WV 26506-6106.
E-mail: dlewelle@wvu.edu

acquired from the hot engine exhausts and from the vortex pair falling through any ambient stratification can dominate the dynamics until the plume mixes sufficiently with the ambient air, typically within one or two Brunt–Väisälä periods (~10–20 min). Finally, at later times, the plume dispersion is dominated by the interaction with the ambient atmosphere, via atmospheric turbulence, gravity waves, and shear. The latent heat release and radiative cooling within the contrail may also contribute significantly at this point as these effects are no longer dwarfed by the wake-induced dynamics. Under favorable conditions (particularly a large ambient supersaturation with respect to ice), the ice mass in the contrail can continue to grow and persist until the individual ice crystals become heavy enough to precipitate out.

In this paper we concentrate on the contrail evolution through the period following its initial formation until the wake motions induced by the aircraft downwash have decayed away—that is, from an age of a few seconds to tens of minutes. We employ large eddy simulations to study the full 3D unsteady wake dynamics in detail during this time period, including a bulk ice microphysics parameterization for the contrail development. This approach is complementary to other recent simulations relevant to contrail development. These include studies of the contrail initiation in the early jet regime (e.g., Kärcher et al. 1996; Kärcher et al. 1998; Brown et al. 1997), others with detailed 3D aircraft wake dynamics but only passive tracers for the engine exhausts (e.g., Lewellen and Lewellen 1996; Gerz and Ehret 1996; Gerz et al. 1998; Lewellen et al. 1998), others more appropriate for studies of older contrails with detailed ice microphysics (in 2D or 3D) but no realistic aircraft wake dynamics (e.g., Gierens 1996; Chlond 1998; Jensen et al. 1998; Khvorostyanov and Sassen 1998), and others with detailed ice microphysics but 2D aircraft wake dynamics (Sussmann and Gierens 1999; Gierens and Jensen 1998), which might reasonably approximate the early vortex and late contrail development but not the transition in between. The wake dynamics alone, ignoring the fate of the engine exhaust products, has also been a significant area for research because of potential effects on closely following aircraft and the resulting safety issues for takeoff and landing at airports. A recent review of these efforts can be found in Spalart (1998); they include some large eddy and direct numerical simulations of the wake vortex dynamics (e.g., Spalart and Wray 1996; Robins and Delisi 1997; Corjon and Poinsot 1997).

Even a casual observer of contrails will have noticed the degree of organized structure often present as a young contrail evolves. Understanding this development is of interest for its own sake, and can provide information about upper-tropospheric conditions as well: the observed contrail development is sensitive to the local relative humidity, turbulence level, wind shear, and temperature stratification, for example. While this provides additional motivation for this work, our main concern here is with a potentially more important issue: whether this early dynamics has any lasting effect on the contrails that persist and grow for long enough time periods to potentially have a climatological impact. There are already some indications from previous work that this might be the case. Studies of passive exhaust tracers (e.g., Lewellen and Lewellen 1996; Gerz et al. 1998) have demonstrated that the vertical extent and distribution of exhaust gases is largely determined by the type of aircraft and its wake vortex dynamics in the first few minutes; for quiet atmospheric conditions the vertical diffusion rate after this period is comparatively slow. Recent 2D case studies by Sussmann and Gierens (1999) have shown that the number of ice crystals present in the contrail can be significantly depleted in response to the wake vortex dynamics, at least for a heavy aircraft (B747) and ambient conditions only slightly supersaturated with respect to ice. We extend these results with our 3D simulations, allowing us to follow the full evolution of the wake even as the vortex pair interacts and decays. As we show below, the ice crystal number depletion can be significant even for smaller aircraft or for sizable supersaturation levels. There has also been a suggestion by Gierens and Ström (1998) that the motions in the aircraft wake may induce significant ice nucleation; we comment below on this possibility as well.

Ultimately, we would like to address questions such as the following. What are the most appropriate starting conditions for contrail studies after the decay of the aircraft wake? In assessing the impact of present and future global air traffic on the total cirrus cloud cover should one assume that the effects scale with the total fuel consumption, the total flight miles, or some more complicated combination involving aircraft type, emission inventories, and atmospheric conditions? Is there any obvious strategy for minimizing persistent contrail production? Our present results shed light on these questions, albeit without providing final definitive answers.

The paper is organized as follows. In section 2 we provide an overview of our large-eddy simulation (LES) model. In section 3 we discuss the procedures used for the contrail simulations, and the conditions simulated. In section 4, we discuss the simulation results, beginning with a review of the basic wake dynamics as illustrated by the simulations, and proceeding to more subtle interactions between the dynamics and contrail development. A summary and some final comments follow in section 5.

2. Model overview

Our principle tool in this study is numerical LES. The range of length scales involved in the decay of an aircraft wake in the atmosphere is much too great to permit a direct numerical simulation of all scales with currently available computer resources. Instead, we solve the Na-

vier–Stokes equations directly for the most important scales in the flow—from well above the cross-stream extent of the wake, to below the scale of the wake vortex core size—but only model the effects of the smaller, unresolved eddies. Details of our LES model applied to aircraft wake dynamics can be found in Lewellen and Lewellen (1996), along with a discussion of the many choices and compromises that must be made to tackle this problem with current computer resources, even within the framework of LES. A summary is given below, followed by a description of the ice microphysics added for the present work.

a. Fluid mechanics

The LES code we employ for aircraft wake simulations was derived from an LES code developed primarily for boundary layer cloud modeling as discussed in Lewellen and Lewellen (1996). It is closely related to the LES model we have used for simulating tornado dynamics (Lewellen et al. 2000). It is a 3D finite-difference implementation of the incompressible Navier–Stokes equations in the Boussinesq approximation, second-order accurate in space and time. It incorporates a piecewise parabolic model (ppm) algorithm for the advection of thermal energy and species concentrations. The pressure field is obtained by directly solving the Poisson equation using fast-Fourier transforms in the downstream direction, the method of Farnell (1980) for nonuniform grids in the cross-stream direction and a tridiagonal solver in the vertical. The Boussinesq approximation was modified to include the buoyancy effects due to acceleration in a strongly rotating flow in addition to the gravitational acceleration.

The primary challenge in these simulations is obtaining adequate resolution together with an adequate domain size. A grid spacing of a few percent of the wing span or less is required to resolve the trailing vortex cores and the transport of the engine exhausts around and into them. On the other hand, line vortices have a sizable long-range influence on the flow-field, so domain widths of several wingspans or more are required to minimize unwanted boundary interactions. We employ three devices to help to meet these conflicting demands: 1) a stretched grid spacing in the vertical and cross-stream directions to achieve fine spacing where it is needed within the wake while maintaining large domain sizes, 2) vertical tracking of the wake to ensure that the fine grid portion of the domain encompasses the falling wake vortices, and 3) different grids (typically 4 or 5) for different segments of the simulations as the wake evolves and the optimum grid requirements change. These are, nonetheless, large computations, employing from 1 to 4.5 million grid points for different segments of the simulations presented here, and typically 6000–8000 time steps. The grids and domains chosen are discussed more in section 3 below. A variable time step was used in the simulations, ranging typically from 0.02 s early on to 1 s for the late stages.

We employ periodic boundary conditions in all three directions. Effectively this means there are neighboring wakes located at twice the distance to the boundary in the vertical and crosswise directions evolving in parallel with our simulated wake. The stretched grid allows us to place the boundaries at sufficient distance to make the effects of these image vortices negligible. Periodicity in the vertical is modified by velocity and temperature shifts between the top and bottom of the domain to permit a mean wind shear and/or stratification to be imposed when desired. The subgrid model utilizes a quasi-equilibrium, second-order turbulence closure scheme with the subgrid turbulent kinetic energy carried as a dynamical variable and the maximum subgrid turbulence length scale related to the numerical grid length. The damping of subgrid turbulence by a stable temperature gradient or a stable rotational velocity field are approximately included via appropriate reductions of the subgrid turbulence length scale. This incorporation of rotational damping effects in the subgrid model [which was employed in Lewellen et al. (1998) but not in Lewellen and Lewellen (1996)] is described in detail in Lewellen et al. (2000). While we believe that such refinements of our subgrid model improve the fidelity of the simulations, they are not crucial to the results presented here. Indeed, the results presented in Lewellen and Lewellen (1996), using of order four times fewer grid points and without the subgrid rotational damping, still compare favorably with the current simulations.

b. Ice microphysics

Given the number of grid points in our simulations, we use a relatively simple (and therefore less costly) bulk ice microphysics parameterization. Four prognostic variables are required: the liquid/ice water potential temperature Θ_{li}; the total water content mixing ratio q_t; the ice mixing ratio q_i; and the ice crystal number density N_i. The physical effects included in the parameterization are diffusional growth/sublimation, sedimentation, buoyancy due to latent heat release, and perturbation pressure effects. In these simulations we have not included ice nucleation, coalescence, radiation, or a multibin ice spectrum.

The diffusional growth/sublimation of the ice crystals is handled at a level similar to Koenig (1971) or Gierens (1996). Starting from the growth rate for an individual crystal (see, e.g., Rogers 1976),

$$\frac{dm}{dt} = 4\pi G(T, P)(S_i - 1)C f_{\text{kin}} f_{\text{ven}}, \qquad (1)$$

we approximate the differential growth contribution to the evolution of q_i as,

$$\frac{dq_i}{dt} = \left[\frac{PD}{RT}(q_v - q_{si})\right] N_i \alpha m^{\beta}, \qquad m = \rho \frac{q_i}{N_i}. \qquad (2)$$

The terms in braces approximate the thermodynamic functions of temperature and pressure $G(T, P)(S_i - 1)$; q_v and q_{si} are the water vapor and ice saturation mixing ratios, and the water vapor diffusion coefficient D is computed as in Hall and Pruppacher (1976). The effects of the crystal shape factor, C; kinetic and ventilation coefficients f_{kin} and f_{ven}; and crystal size spectrum are included (to the extent they appear at all) in the choice of α and β. For our simulation condition of $T = 220$ K and $P = 250$ hPa (see below) we choose $\alpha = 11.0$ and $\beta = 0.45$ to agree with the rates given by Gierens (1996) (who assumed small columns for the crystal shapes) for these conditions. The resulting growth rates agree to within 15% of those obtained using the kinetic and ventilation factors from Stephens (1983) and spherical crystals for radii between 2 and 40 μm.

Here N_i is treated as a locally conserved quantity unless $\Delta t dq_i/dt + q_i$ becomes less than or equal to zero at some point in the evolution (for numerical time step Δt), whereupon N_i within that grid cell is set to zero and those crystals are permanently lost. The N_i evolution within the contrail remains fairly smooth despite this all or nothing grid cell sink because of the fine grid resolution employed and the importance of turbulent mixing averaging neighboring grid cell populations. For this purpose (as well as the implementation of precipitation given below and particle size diagnostics given later in the paper) we are effectively treating the ice crystal spectrum within a single grid cell as monodisperse. Improving upon this in a bulk parameterization used with fine grid resolution is problematic without increasing the number of degrees of freedom in the parameterization: any assumed spectral shape would not be preserved by local turbulent mixing. Nor is it clear what spectra would be appropriate locally: aircraft measurements of ice crystal spectra in contrails are composites, involving a spatial average over local populations that can individually have quite different spectra. As we discuss in the results below, the ice crystal number densities in our simulations are large enough that near-equilibrium ($q_v \approx q_{si}$) conditions occur almost everywhere. Thus while the treatment in (2) and of the evaporative loss of N_i are admittedly rather crude, the sensitivity of the young contrail's evolution to the choice of parameterization is not as important as it otherwise might be.

The gravitational settling velocity, V_{fall}, is computed at a similar level of approximation,

$$V_{\text{fall}} = am^b. \tag{3}$$

We have chosen a and b so that the results agree with the parameterization of Böhm (1989) for the limit of small spherical particles. For the conditions of our simulation, this is $a = 6.66 \times 10^5$, $b = \frac{2}{3}$ (giving V_{fall} in m s^{-1} for m given in kg). For most of our simulations the effect of precipitation is negligible; only for the largest supersaturations we consider do the fall velocities begin to compete with the fluid velocities in our simulations and even then only toward the end of the simulation period ($\sim$30 min).

We compute q_{si} from Θ_{li}, and P using the same saturation formulas as Chlond (1998). The one difference in the treatment is that we include the pressure perturbations due to the fluid dynamics. For a heavy transport aircraft this can be a significant effect in the cores of the wing tip vortices.

Since we must include buoyancy effects for the ambient stratification and the heat in the engine exhausts, we include the buoyancy from the release of latent heat upon freezing, but it does not represent a significant effect for young contrails. In his simulations with large supersaturation with respect to ice of 129%, Chlond (1998) finds peak velocity scales of order 0.1 m s^{-1} driven by the latent heat release after timescales of several minutes. This is well below the turbulent velocities induced by the wake downwash and the Brunt–Väisälä oscillations which follow. We have not included radiative emission and absorption from the ice cloud at all. According to Chlond their impact is small even compared to the latent heating effects. Gierens (1996) concludes similarly that the radiative cooling has little effect on the dynamics in the first 30 min.

Our omission of ice crystal nucleation deserves comment in light of the conjecture in Gierens and Ström (1998) that nucleation induced by aircraft-generated upward circulations might be important. The fluid motions in the aircraft wake are primarily downward, in an ellipse of fluid surrounding the vortex cores. The secondary, upward recirculations outside of this ellipse give rise to vertical displacements equal to the height of the ellipse or less—that is less than or of order half of the vortex pair separation. For a heavy transport such as a B747 this amounts to 25 m or less (a result we have checked by following a large sample of Lagrangian trajectories within a wake simulation). For highly supersaturated conditions this displacement could induce ice nucleation; however, in general one would expect vertical displacements of this order or greater to be present already from the ambient atmospheric waves/turbulence. In other words, if the supersaturation level is high enough that the small upward displacements produced by the aircraft would induce ice nucleation, then the ambient waves/turbulence likely would as well, resulting in the presence of natural cirrus. The window of atmospheric conditions for which the wake motions induce ice nucleation but natural cirrus is absent is thus likely to be a narrow one, which we do not treat here. The upward displacements later in the evolution due to wake-induced Brunt–Väisälä oscillations can be larger, but involves primarily fluid mixed with the exhausts, that is, where ice crystals are already present and scavenging the available moisture. The effects of natural cirrus on contrail evolution (and vice versa) have to our knowledge not yet been treated in the literature and are outside the scope of our present simulations as well. It is likely, however, that the ice mass would be reduced:

TABLE 1. Fixed simulation parameters for representative cruise conditions in the upper troposphere, including the vortex separation (b_0), circulation (Γ), aircraft mass, engine position from the centerline as a fraction of the distance to the vortex, fuel flow rate, flight speed (U), engine heat per meter of flight path ($\int \Delta\Theta$), integrated total water emitted per meter of flight path ($\int \Delta q_t$), integrated momentum in the exhaust jets per meter of flight path ($\int \Delta V$), temperature, pressure, lapse rate ($d\Theta/dz$), and turbulent dissipation rate (ϵ).

Aircraft	b_0 m	Γ $m^2\ s^{-1}$	Mass kg	Eng. pos. d_{eng}/d_{vtx}	Fuel flow kg km^{-1}	U m s^{-1}	$\int \Delta\Theta$ K m^2	$\int \Delta q_t$ g kg^{-1} m^2	$\int \Delta V$ $m^3\ s^{-1}$
B747	47	670	314 000	0.48, 0.83	12	247	909	37.9	1620
B737	22.3	220	47 000	0.44	2.5	238	189	7.89	341

Atmosphere: $T = 220$ K, $P = 250$ hPa, $d\Theta/dz = 2.5$ K km^{-1}, $\epsilon \sim 1.5 \times 10^{-5}$ $m^2\ s^{-3}$

with the available moisture already taken up by the natural cirrus, the contrail crystals would remain small and more easily evaporate away due to the adiabatic heating induced by the vortex descent (which likely removes some of the natural cirrus as well).

3. Simulation conditions

There is, of course, an enormous range of atmospheric conditions encountered by many different types of aircraft; we cannot hope to fully explore this parameter space in the present work. We confine ourselves to a handful of simulations for fairly ''typical'' conditions. These are summarized in Tables 1 and 2.

Consider first the aircraft-related conditions. We have chosen the B747 and B737 from the range of commercial aircraft because they represent common examples from different ends of that spectrum: a large four-engine and smaller two-engine transport, respectively. We consider only cruise conditions in the upper troposphere where persistent contrails are most likely. For our initial conditions we include a portion of the wake as if it were laid down instantaneously within our domain. This is an appropriate approximation here given the rapid aircraft flight speed and our starting point a few seconds after the aircraft has past.

Some properties of the initial cross sections of the wake are summarized in Table 1. The downward momentum imparted to the vortex pair supports the weight of the aircraft in level flight. Accordingly, the vortex separation, b_o, circulation about the vortices, Γ, aircraft mass, M, and flight speed, U, are related by $gM = \rho\Gamma b_o U$ (with g and ρ the gravitational acceleration and air density, respectively). The mass of the aircraft can vary significantly during a long flight as fuel is consumed; those given in Table 1 are chosen to be representative midrange values. The heat produced by the engines per meter of flight path, $\int \Delta\Theta$, was computed using the chosen fuel flow rates, a specific combustion heat of 43 MJ kg^{-1} appropriate for kerosene type jet fuels, and an assumed jet engine efficiency of 30%. The integrated total water emitted per meter of flight path follows from the fuel consumption and an emission index of 1.25 kg kg^{-1}. The integrated momentum in the exhaust jets is that appropriate for a thrust computed using a specific fuel consumption of 18.7 mg $N^{-1}s^{-1}$. The cross-stream distributions of the velocity fields and exhaust products depend on the rollup of the vorticity shed from the wing and were taken from a UNIWAKE simulation (Quackenbush et al. 1996), with values scaled so as to match the desired integrals in Table 1.

TABLE 2. Principle simulations.

Simulation	Aircraft	RH_i	EI_{iceno} (kg^{-1})	Comments
A30	B747	130%	10^{15}	
A30b	B747	130%	10^{15}	Double domain
A30c	B747	130%	10^{15}	Shear = 0.001 s^{-1}
A20	B747	120%	10^{15}	
A10	B747	110%	10^{15}	
A10b	B747	110%	3.7×10^{13}	
A10c	B747	110%	10^{12}	
A10d	B747	110%	10^{15}	Shear = 0.01 s^{-1}
A2	B747	102%	10^{15}	
B30	B737	130%	10^{15}	
B10	B737	110%	10^{15}	
B2	B737	102%	10^{15}	

The initial formation of the contrail is a complex and not completely understood problem (see, e.g., Kärcher et al. 1996), which we make no attempt to treat here. At the few second point where we pick up the wake, the contrail is already formed if conditions are favorable (see, e.g., Schumann 1996). We take the ice crystals, then, as given, with a distribution following that of the engine exhausts and a total number density given by an effective ice crystal number emission index, EI_{iceno}, together with the fuel flow rate. At the time of his review, Schumann (1996) quoted an uncertainty in EI_{iceno} from the literature ranging from 10^{11} to 10^{15} kg^{-1}. Recent in situ measurements, however, are consistent with a value of around 10^{15} kg^{-1} (Schröder et al. 2000; Anderson et al. 1998). We choose this value for most of our simulations (Table 2); this agrees with the values chosen in recent work by Sussmann and Gierens (1999) and Gierens and Jensen (1998). In order to have some measure of the sensitivity of our results to the value of EI_{iceno} (which it may prove possible to vary by altering fuel composition or engine performance) we chose two smaller values in simulations A10b and A10c. That used in A10b is consistent with that used in the earlier studies of Gierens (1996) and Chlond (1998); that of A10c is toward the low end of the range quoted in Schumann (1996).

The large magnitude of EI_{iceno}, and small initial contrail size, translates into large number densities in the early contrail. Because of this, the choice of the initial ice mixing ratio (q_i) distribution is not crucial; the ice quickly adjusts to the local equilibrium conditions. We choose initial distributions for q_i proportional to the engine exhausts for simplicity. This implies that all of the ice crystals at our starting time are the same size.

To complete the initial conditions for our simulations, the aircraft wake is superimposed with an ambient atmospheric field, as described in Lewellen and Lewellen (1996). The atmospheric conditions we have chosen to keep fixed, listed in Table 1, are within the range appropriate for the upper troposphere; they coincide with the values used by Chlond (1998). The atmospheric turbulence fields used were themselves results of separate large-eddy simulations. Fields with the desired stratification, wind shears, and domain sizes were given relatively large initial velocity and temperature perturbations, and their evolution followed via LES until the turbulence and gravity waves had a chance to adjust to the stratification and shear, and their amplitude had decayed into a desirable range. For the current simulations we chose what we would consider modest levels of turbulence for cruise flight conditions, with initial turbulent dissipation rates in the ambient fields (for cases without shear) of order 1.5×10^{-5} m^2 s^{-3}.

The principal atmospheric property varied in our simulations is that with the most direct and dramatic effect on the aircraft contrail: the ambient relative humidity with respect to ice, RH_i. For any given simulation we have chosen this to be constant within our domain (apart from a level set by the turbulent fluctuations in the field). We could as well have chosen a constant total water mixing ratio, constant relative humidity with respect to water (as in Chlond 1998; Gierens 1996), or a nontrivial vertical gradient (as in the case studies of Jensen et al. 1998; Khvorostyanov and Sassen 1998; Sussmann and Gierens 1999; Gierens and Jensen 1998). These and other possibilities can all reasonably occur in the atmosphere over regions of a few hundred meters depth, which are relevant here. We confine ourselves to $RH_i > 100\%$ in order to obtain persistent contrails, taking values from 102% to 130%. Recent observational studies suggest that supersaturations of 130% or greater with respect to ice in cloud-free air are not uncommon in the upper troposphere (Heymsfield et al. 1998).

Table 3 summarizes the grids employed for sample simulations for each aircraft. These are representative of those for all of the simulations save a few exceptions: the downstream domains for run A30b were twice as large as in Table 3 but with essentially the same resolutions; the domains for run A10d were extended significantly in the cross-stream direction to adequately contain the wake plume as it was smeared by the cross-stream wind shear. The choice of grid for a given segment of a simulation was correlated with the wake vortex dynamics then occurring in order to best apportion the limited number of grid points available given the physics that had to be resolved. As the wake velocities decay and the contrail expands, less grid resolution is required, but the relatively fine grid must cover a larger volume. Accordingly we interpolated the species and flow fields to new grids when it appeared beneficial during a simulation. In several cases simulation segments were run both on the old and new grids and the results compared to confirm that the coarser grids were still faithfully resolving the most important dynamics. Typically the first grid was used when the vortex cores were tightest and the vortex evolution largely two-dimensional (varying little downstream), the second during the vortex linking and reconnection phase, the third as the vortex rings oscillate to expand significantly in the cross-stream direction before finally decaying, and the last grids as the Brunt–Väisälä sloshing of the wake and atmospheric turbulence dominates the dynamics. These basic features of the wake dynamics are discussed more below. After the simulation segments on the first three grids were performed (typically 240 s of simulated time for the B747 cases, 200 s for the B737 ones) the domain size was doubled for the remainder of the simulation. To do this the final field generated on the third grid was periodically doubled in the downstream direction and added to an ambient turbulence field generated by a separate LES on the doubled domain.

As discussed below, the basic wake decay via the Crow instability is periodic in the downstream direction. This periodicity must be commensurate with the downstream domain size in our simulations and thus influences the choice of domain size. This issue is discussed at length in Lewellen and Lewellen (1996). For a given aircraft, there is considerable variability in the observed periodicity, depending on the wave and turbulence spectrum in the ambient atmosphere. It is not unusual to see

TABLE 3. Sample grids for B747 simulations (top set) and B737 simulations (bottom set). Domain dimensions are in kilometers and grid spacings in meters for the (cross-stream) × (vertical) × (downstream) directions, respectively.

Grid	1	2	3	4	5
B747: Domain	1 × 1.2 × 0.3	1 × 1.2 × 0.3	1 × 1.2 × 0.3	2 × 2 × 0.6	
Grid points	118 × 110 × 82	120 × 121 × 162	152 × 127 × 130	104 × 122 × 122	
Fine spacing	1.2 × 1.2 × 3.75	1.7 × 1.7 × 1.88	2.3 × 2.3 × 2.3	5 × 5 × 5	
B737: Domain	0.5 × 0.62 × 0.16	0.5 × 0.62 × 0.16	0.5 × 0.62 × 0.16	1 × 1 × 0.32	1 × 1 × 0.32
Grid points	126 × 114 × 82	120 × 117 × 162	152 × 122 × 130	104 × 122 × 122	132 × 138 × 66
Fine spacing	0.6 × 0.6 × 2	0.8 × 0.8 × 1	1.25 × 1.25 × 1.23	2.5 × 2.5 × 2.66	5 × 5 × 5

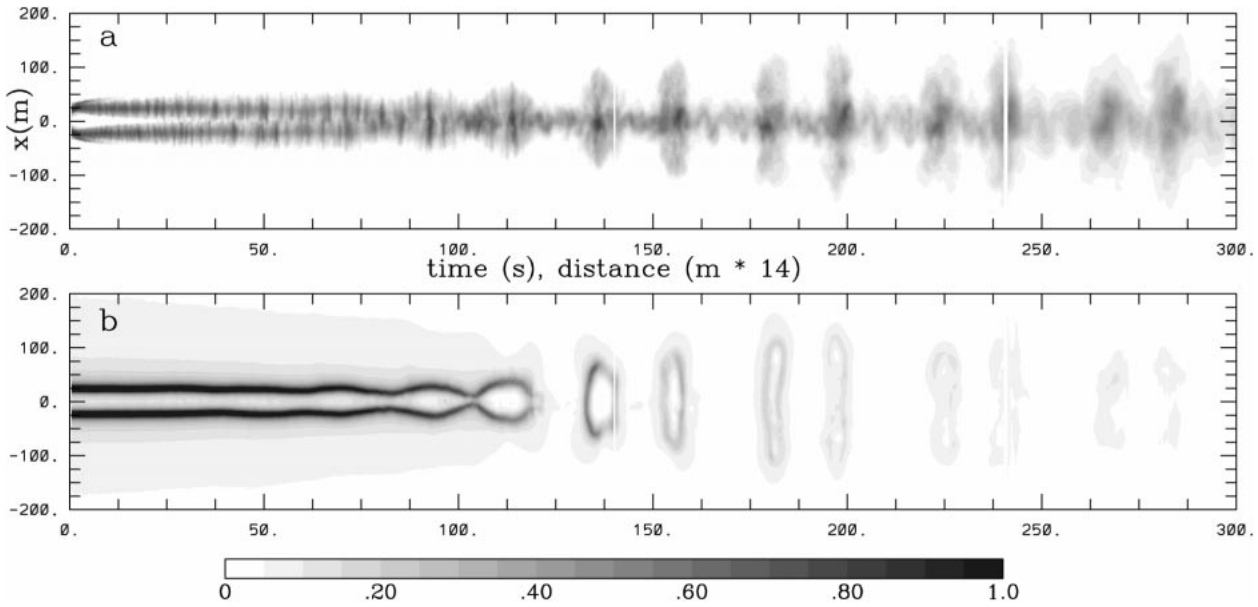

FIG. 1. Downstream space/time vs width plot of vertically integrated fields for a simulated B747 contrail with $RH_i = 130\%$ (simulation A30b). (a) Integrated ice crystal number density in 4×10^{11} m^{-2}; (b) integrated perturbation pressure in -10^3 Pa m.

a factor of two variation in period within a single contrail in the sky. For this work the B747 domains were chosen commensurate with a wavelength of 300 m. The ratio of wavelength to vortex separation is in the most favored range found in the DNS study of Spalart and Wray (1996); this is about 25% less than the wavelength of maximum amplification deduced in Crow (1970). We choose the B737 domains commensurate with a wavelength of 160 m, as in Lewellen et al. (1998), where the wavelengths were measured (using LIDAR) from a particular set of B737 flight tests. Nondimensionalized by the vortex separation, this value falls in between that of Crow (1970) and Spalart and Wray (1996).

In previous work [e.g., simulations of the case presented in Lewellen et al. (1998) including 1, 2, 3, and 4 periods within the domain], we have found little variation of the basic wake decay with downstream domain size. Doubling or even quadrupling the downstream domain, doubles or quadruples the number of Crow periods realized within the domain but effects little if any change in the rate of wake dispersion, overall vertical and horizontal extent, wake lifetime, etc. Accordingly, in all the simulations here with the exception of A30b, we have realized only a single period of the Crow instability within our domain for the first three segments of each simulation.

4. Results

a. Review of basic wake decay mode

Figures 1 and 2 illustrate some of the basic wake dynamics out to an age of 5 min for simulation A30b, a B747 with large ambient ice saturation (130% relative humidity with respect to ice). The format is as described in Lewellen et al. (1998), inspired by scanning lidar measurements of wakes. The wake is sampled as if it were being advected at a steady rate by a mean wind aligned with the contrail [as was the case for the lidar measurements discussed in Lewellen et al. (1998)]. The horizontal axis in each case then varies over time as well as downstream distance so that both the temporal evolution and spatial structure can be seen. The ''drift velocity'' determining the unit of distance per unit of time has been chosen to be 14 m s^{-1}, which is in a convenient range for displaying both the temporal and spatial structure.[1] Figure 1 is a view from below with the fields vertically integrated; the low pressure centers in the second panel provide a good view of the trailing vortex dynamics. Figure 2 is a view from the side with the fields integrated in the cross-stream direction. The horizontal and vertical lengths in Fig. 2 are displayed at the same scale. In Fig. 1 the cross-stream dimension has been expanded by a factor of 3 relative to the downstream direction to better display the dynamics; the appearance in the sky would be correspondingly thinner and more stretched out than is apparent in the figure.

The main features of the wake evolution can be observed in these figures. Initially the vortex pair descends rapidly. Perturbations of the vortices from the ambient atmosphere (and/or unsteady wing loading or jet tur-

[1] A much higher velocity would sample the spatial structures repeatedly before they underwent much temporal evolution; a much lower velocity would sample the structures so slowly that a great deal of temporal evolution would take place in between subsequent samplings and be missed.

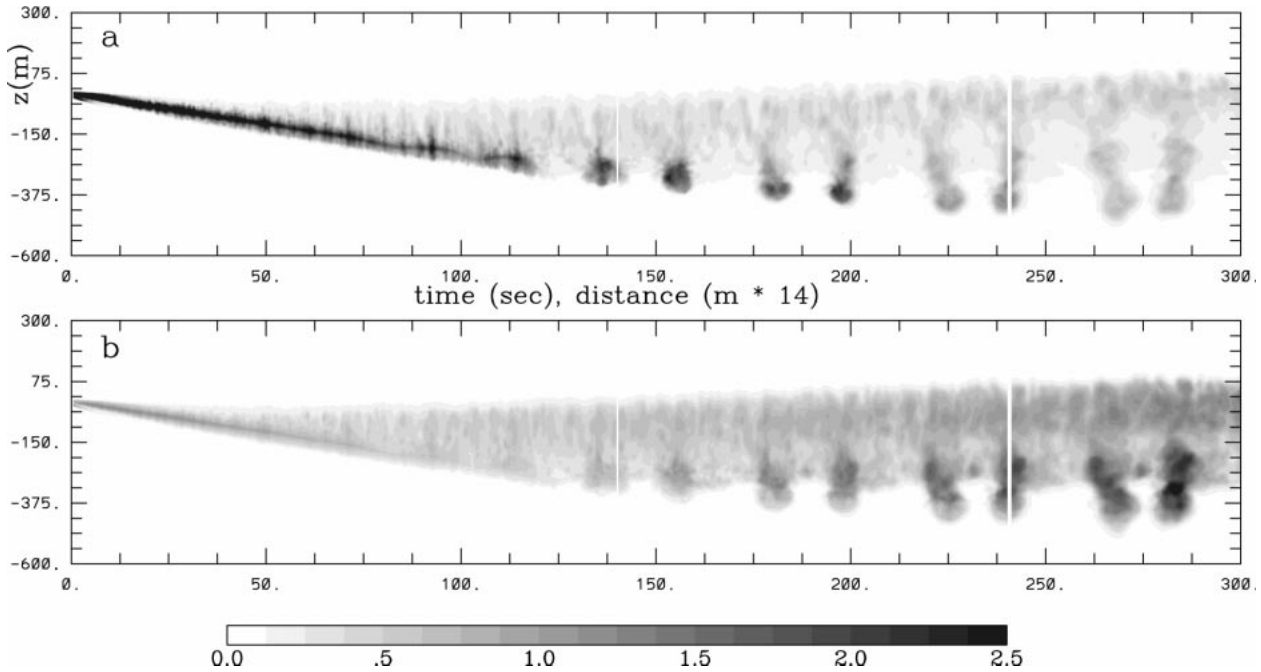

FIG. 2. Downstream space/time vs height plot of cross-stream integrated fields for a simulated B747 contrail with $RH_i = 130\%$ (simulation A30b). (a) Integrated ice crystal number density in 10^{11} m^{-2}; (b) integrated ice mass density in g m^{-2}.

bulence) grow in a sinusoidal mutual inductance instability (the Crow instability). The early growth of this instability is well understood. To a good approximation (as long as the ambient shear is not too large) we can view the wake as a pair of line vortices in an otherwise vorticity free field. The velocity field advecting each vortex can then be thought of as a sum of two parts: the velocity field induced by the neighboring vortex (''mutual induction''), and that induced by itself (''self induction''). The former produces the rapid descent of the vortices at an initial velocity of $\Gamma/2\pi b_0$. If the vortices are perturbed sinusoidally, then this mutual induction drives the segments of the vortices that are closest together down the fastest. At the same time, however, the self induction arising from the perturbation of the vortex tends to rotate it about its axis in the opposite direction. The net effect is that the sinusoidal perturbation rotates neither clockwise nor counterclockwise but aligns itself in a plane at a 45° angle to that containing the vortex pair, and its amplitude grows exponentially. The rate of growth depends on the wavelength of the perturbation as well as the vortex spacing and circulation [and to a lesser extent core size, axial velocity, etc. (see, e.g., Bliss 1982)]. In a turbulent atmosphere the vortices see a superposition of ''sinusoidal perturbations,'' and the instabilities for different wavelengths compete with each other. Those that are in the range of most rapid growth and have the largest initial perturbations eventually win out.

The growth of the Crow instability proceeds until the vortices touch, reconnect, and form elongated vortex rings. These open up and then elongate in the cross-stream direction (under the action of the velocity induced by the curvature of the ring out of the plane of the original two vortices), and further interact with themselves, even sometimes relinking again to form two rings from one. During this entire evolution the vortex cores are continually diffusing due to the smaller-scale atmospheric turbulence and interaction with the ambient stratification. At the turbulence levels of the present simulation the rings self-interact and finally dissolve not long after their transverse oscillation. During their lifetime the rings continue to drop, giving rise to the periodic series of puffs often seen in contrail evolution.

In the present case the descent of the vortex rings (or their remnants) continues until an age of approximately 300 s with about half of the total wake descent (of ~400 m) occurring after the pair initially touches at an age of about 100 s. In general the basic length and timescales for the Crow instability may be taken as the vortex separation, b_0, and the fall time, $t_f = 2\pi b_0^2/\Gamma$ (i.e., b_o divided by the initial vortex pair fall velocity). The onset of the pair linking occurs at an order of 3–6 fall times (depending on the initial perturbations inherited from the atmosphere); the final dissolution of the vortex system at an order of 10–20 fall times after a total wake descent of order $6–12b_o$ (both depending on ambient turbulence levels and stratification, among other variables).

The coherent wake dynamics does not end with the dissolution of the wake vortices. The positive buoyancy acquired by the vortex system's descent through the stratified atmosphere (together with the heat in the initial engine exhaust), drives a strong Brunt–Väisälä oscil-

lation. In the absence of significant wind shear, we find that this oscillation drives the dominant turbulence, which mixes the wake plume until it damps, after one to three Brunt–Väisälä periods, to the level of the ambient atmospheric turbulence.

The wake dynamics is easy to follow given the velocity and pressure fields from the simulation. It is much less clear from observations of condensation trails, for two reasons. First, the engine exhausts do not all neatly follow the vortex cores. Second, the contrail ice is by no means a passive tracer; it has significant dynamics of its own. We consider these effects now in turn. At the large value of ice supersaturation of simulation A30b, the ice crystal number density behaves like a passive scalar originating with the engine exhausts. Early in the wake evolution the exhausts follow one of three basic types of trajectories. Some is captured within the trailing vortex cores where its subsequent mixing and dilution is suppressed. Some remains outside the vortex cores but within the ellipse of fluid descending with the vortex pair; this fluid mixes efficiently within the ellipse but only weakly with the fluid outside. Finally, some of the exhaust is not captured at all, following a trajectory outside of the ellipse of fluid as the vortices roll up, and is left behind at the flight level. The main factor determining the fractions of exhausts following each trajectory is its initial placement. We have examined this in simulations (not presented here) using passive tracers introduced in different locations. Exhausts originating near the wing tips were entirely captured within the vortex cores; for tail exhausts somewhat more than half escaped the vortex system entirely, with the rest mixed across the ellipse of descending fluid. Exhausts originating from the wing nearer to the fuselage (e.g., from the inboard engines of the B747) are mostly captured within the ellipse and vortex cores, with only a small fraction escaping entirely (although this fraction increases with increasing ambient turbulence or stratification).

As the vortices fall, some exhausts from the outer edge of the ellipse are typically detrained to form a thin vertical curtain between the flight level and the vortices. Within the vortex cores small axial pressure variations (due to ambient turbulence) can lead to strong downstream variations in exhaust concentrations—sometimes misrepresented as being due to vortex ''breakdown'' or ''bursting.'' When the vortices link to form rings, some of the fluid escapes and rises to join with the upper wake. The exhausts within the cores are strongly scrambled during the linking process, so that they do not represent a reliable signature for the vortex dynamics, as is clear from Fig. 1. This led in earlier observations of the Crow instability using smoke tracers to the belief that the coherent vortex dynamics suddenly ends shortly after the members of the vortex pair first touch. This picture, sometimes used to try to extend the region of validity of 2D simulations, is not borne out by fine-resolution 3D results.

The ice mass evolution for highly supersaturated conditions (Fig. 2b) differs from the dispersion of a passive tracer chiefly because the dominant source of moisture is not the engine exhausts, but the ambient atmosphere. Accordingly, the ice mass tends to grow with the volume of the plume, with its value set by the excess moisture above the ice saturation level. The spatial structure at a given time in Fig. 2b arises mainly from the cross-stream integration over the shape of the plume volume rather than from large variations of the ice mass density within the plume.

Figure 3 shows a downstream space–time slice (rather than the cross-stream integration as in Fig. 2) for simulation A30b. The position of the slice in the cross-stream direction has been chosen midway between one of the vortex cores and the aircraft center line. The mean crystal diameter (assuming spherical crystals) in the bottom panel shows the expected inverse relationship between crystal size and number density. Accordingly, the crystal size in different regions of the contrail can vary significantly, with in general much larger crystals in the upper wake than in the lower. The ratio of the actual ice mass to the local equilibrium value {i.e., $q_i/[q_{si}(\mathrm{RH}_i - 1)]$} in the top panel shows that the ice plume is near equilibrium almost everywhere. The exceptions are the plume edges, where the crystal numbers fall off, and, more interestingly, in the rapidly descending vortex system. As the fluid around the vortices falls it is adiabatically compressed by the increasing ambient pressure level. The accompanying rise in temperature lowers the relative humidity in this fluid so that the existing ice mass is above the now lowered equilibrium level. At high ambient humidity levels this effect has no lasting consequences, but at lower levels it can dramatically effect the contrail evolution, as we discuss in detail below.

The visual appearance of a contrail does not coincide with either the ice crystal number density distribution, or the ice mass distribution, but depends as well on other factors such as the crystal size and shape and the angle of the sun. The rate of scattering and absorption per unit volume of contrail is more closely represented, for visual wavelengths and small crystals, by the total crystal surface area per unit volume.[2] Figure 4 displays a 3D isosurface of surface area density for simulation A30b at time 240 s, giving some indication of the visual appearance of this contrail at this stage of development. Note that strong ambient stratification is not required for the appearance of the periodic downward puffs generally present in contrail development, as is often stated in popular literature (e.g., Schaefer and Day 1981). This

[2] In this regime the extinction per mass of ice crystals scales approximately as the inverse crystal radius (see e.g., Ebert and Curry 1992). Multiplied by the ice mass per air volume to obtain the extinction per contrail volume, this results in the scaling with total surface area density.

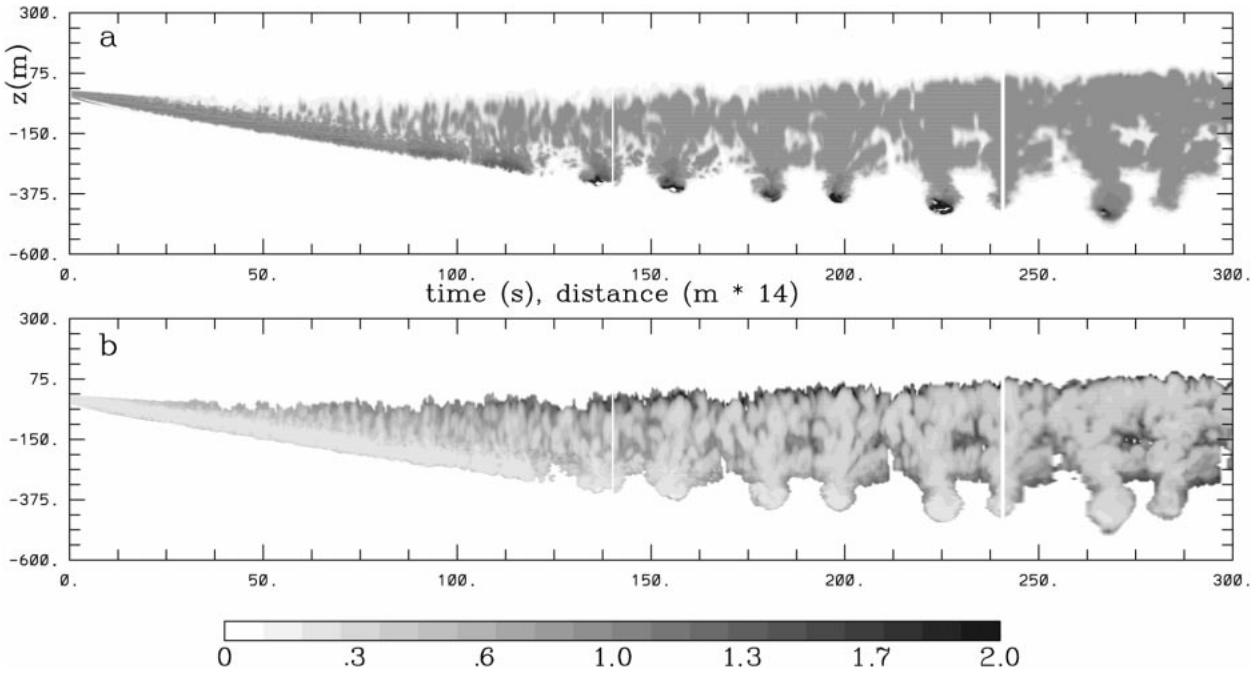

FIG. 3. Fields on a downstream space/time vs height slice for a simulated B747 contrail with $RH_i = 130\%$ (simulation A30b). (a) Here (ice mass)/(equilibrium ice mass); (b) effective ice crystal diameter in 10-μm units.

belief probably dates back to an earlier explanation for these puffs due to Scorer and Davenport (1970).

b. Varying RH_{ice} and aircraft type

Figure 5 illustrates results for simulation A10 analogous to those in Fig. 2. The conditions are the same as before except the ambient relative humidity with respect to ice is now 110% (and 10 min of simulated results are shown). The compressional heating now leads to the eventual evaporation of the ice crystals within the immediate vicinity of the vortices. This effect was first noted in the literature by Sussmann and Gierens (1999) in the context of two-dimensional simulations with low ambient ice supersaturations. In three dimensions we can carry the simulations past the vortex linking stage to find that this can be an important effect even for significant ambient ice supersaturations largely because of the significant vertical descent of the wake occurring after linking. The evolution of the ice crystal number density is now quite different than that of a passive tracer.

The fraction of ice crystals lost through this mechanism depends on a competition between the rate at which the fluid around the vortices is forced below the saturation level (and the ice crystals sublimate), and the rate at which supersaturated ambient fluid is mixed into this system. For the conditions considered here (there is a modest dependence on ambient temperature) a parcel with initial $RH_i > 1$ would, in the absence of mixing, become subsaturated after descending approximately $920(RH_i - 1)$ meters.[3] The mixing that occurs into the ellipse of descending fluid increases the required drop significantly; for example, for case A10 the rate of ice crystal loss is largest at about 95 s after a drop of 215 m, rather than at 40 s after a drop of 92 m. The loss of ice crystals within the vortex cores themselves are slowed by two other factors—the enhanced humidity from the engine exhausts confined there and the lowering of the saturation point due to the lower pressure within the cores. For the present B747 simulations the added pressure drop in the vortex cores is 2.4 hPa early in the evolution, 1.3 hPa at 60 s, and 0.63 hPa at 100 s. It is the lower core pressure that makes the contrail a good signature for the vortex dynamics for some favorable conditions (e.g., Fig. 13 below) and, together with the adiabatic heating, leads to the contrail pair becoming progressively thinner over time in these cases (cf. Fig. 3 in Sussmann and Gierens 1999).

For supersaturated conditions the future of any ice crystals is assured if they can escape from the descending vortex system. Any enhancement to mixing improves their prospects. Accordingly there are two particularly important events during the wake evolution. First the initial vortex linking process, which is invariably associated with the escape of some of the exhaust from the descending vortex system as well as a dilution

[3] This is arrived at by equating the initial $q_{si}RH_i$ with the q_{si} after an adiabatic parcel descent of δz meters, expanding the saturation formula in powers of δz and solving to leading order.

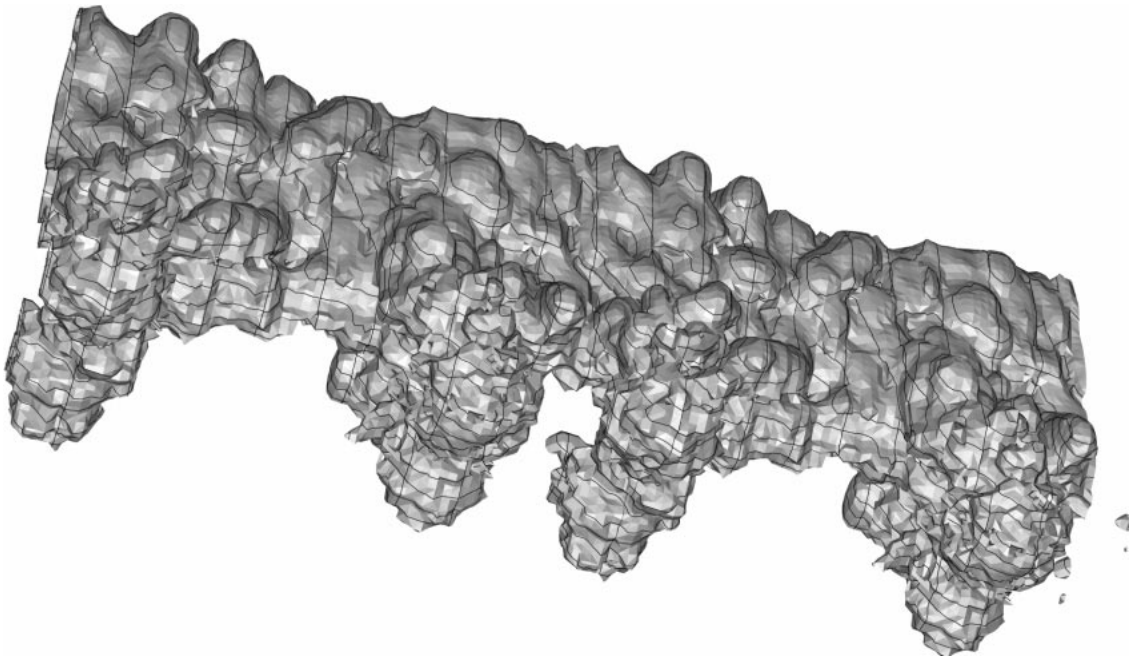

FIG. 4. Three-dimensional isosurface of ice crystal surface area density = 0.005 m^{-1} for a simulated B747 contrail with RH_i = 130% (simulation A30b) at an age of 240 s. The downstream domain length shown is 1200 m.

within the vortex cores, and second, the final collapse of the coherent vortex rings, after which the once confined ice crystals efficiently mix with the ambient atmosphere and begin to buoyantly rise.

Figure 6 illustrates results analogous to those in Fig. 5 but for a B737 [with the drift velocity taken to be 7.62 m s^{-1} as in the results presented in Lewellen et al. (1998)]. In this case with a smaller aircraft (whose vortices fall neither as far nor as fast) the ice crystal loss is much less, and the contrail retains the full plume

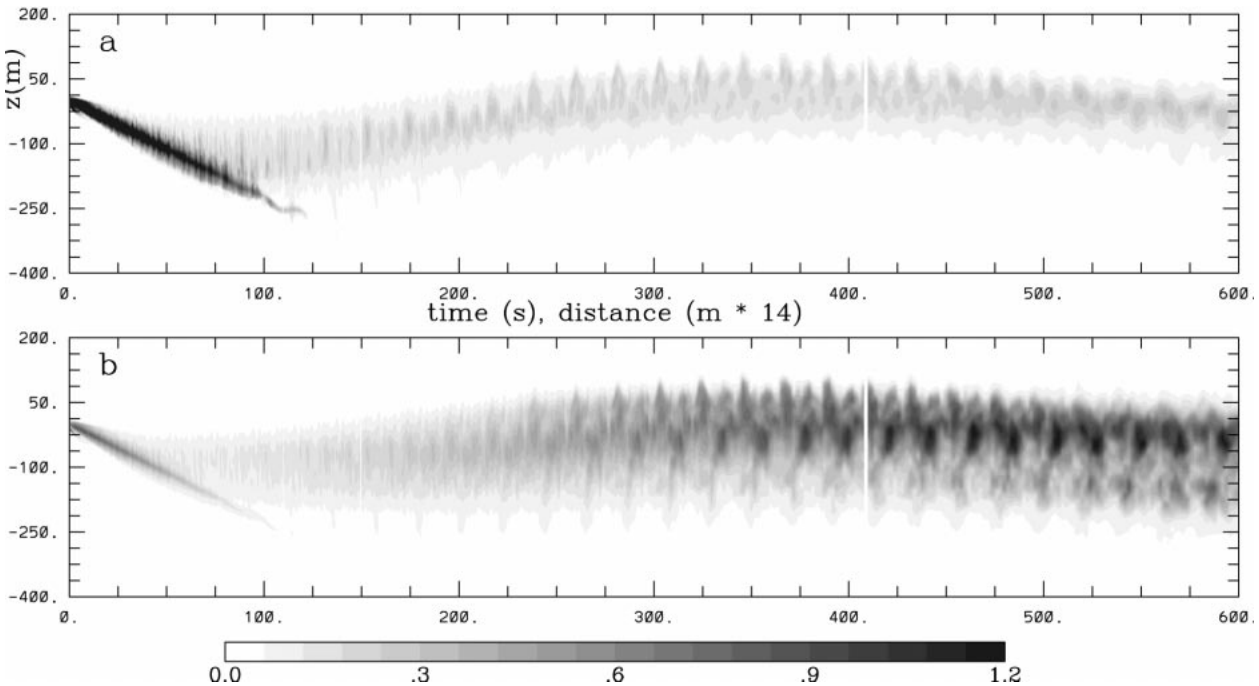

FIG. 5. Downstream space/time vs height plot of cross-stream integrated fields for a simulated B747 contrail with RH_i = 110% (simulation A10). (a) Integrated ice crystal number density in 2×10^{11} m^{-2}; (b) integrated ice mass density in g m^{-2}.

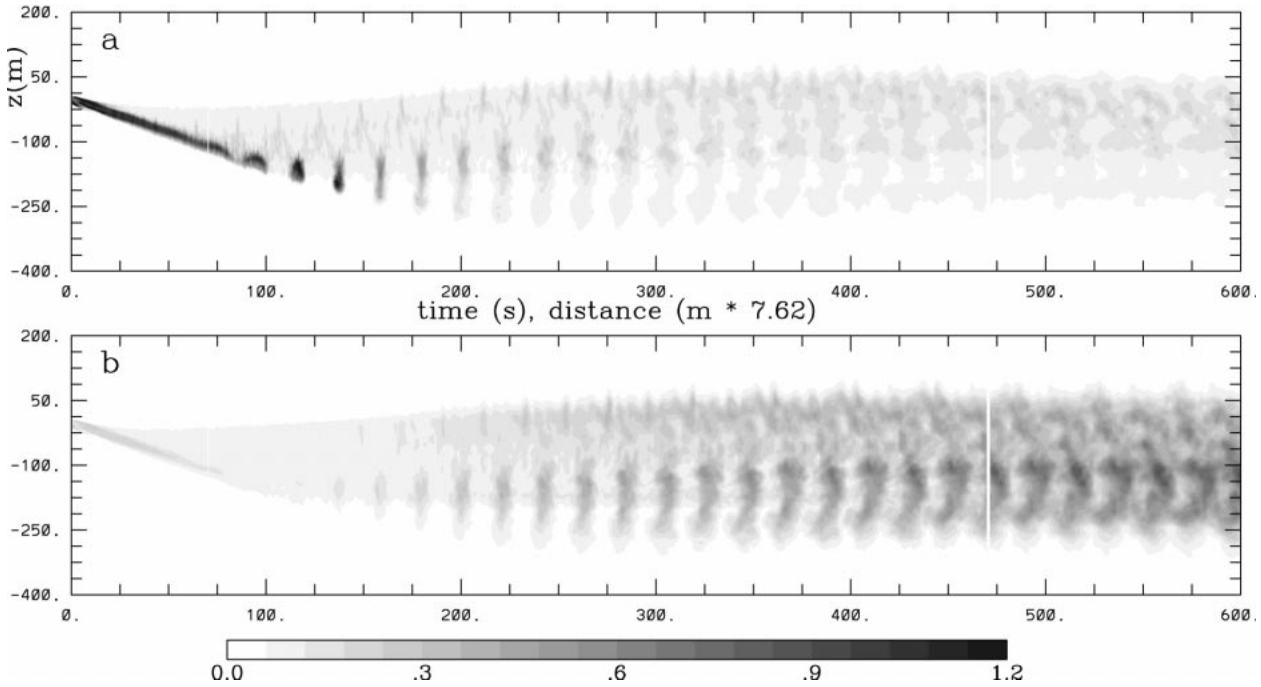

FIG. 6. As in Fig. 5 but for a B737 contrail (simulation B10).

volume. A lesser contributing factor is that the engines are further inboard so that more of the exhaust is detrained into the upper wake and less is confined within the vortex cores.

Figures 7–9 summarize some results from our simulations varying RH_i for the two chosen aircraft. One should keep in mind that these are based on single realizations of short lengths of contrails; however, there is some indication that for integrated quantities the variation between different turbulent realizations under similar conditions is not great. For example, the results for simulations A30b and A30c are indistinguishable on these plots from those of simulation A30. The total ice crystal surface area (computed here assuming spherical crystals) is important for heterogeneous chemistry in the contrail, as well as for its influence on the contrail's radiative properties. The increase in total ice mass, surface area, and the fraction of ice crystals surviving, is evident as the ambient relative humidity with respect to ice is increased. More surprising are the differences between aircraft. While the B747 contrail has a larger total ice mass than the B737 for high ambient supersaturations, we have for $RH_i = 110\%$ that the B737 eventually produces as significant a contrail as the B747 even though it consumes only about 20% as much fuel per meter of flight path. The fraction of ice crystals lost due to adiabatic heating is greatest when the evaporation occurs before the onset of vortex linking (B747, $RH_i = 102\%$), less but still more than two-thirds of the total when it occurs during the linking process (B747, $RH_i = 110\%$; B737, $RH_i = 102\%$), only a modest fraction when it occurs after linking (B747 $RH_i = 120\%$; B737, $RH_i = 110\%$), and nonexistent if it does not arise before the vortex rings dissolve ($RH_i = 130\%$).

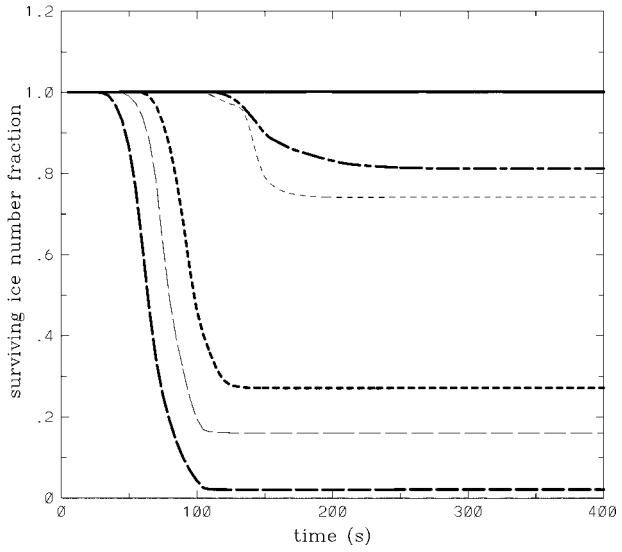

FIG. 7. Fraction of initial ice crystal number surviving vs time. Thick lines indicate B747 contrails, thin lines B737. Here $RH_i = 130\%$ (solid lines), $RH_i = 120\%$ (long-short dash), $RH_i = 110\%$ (short dash), and $RH_i = 102\%$ (long dash).

We note in passing several other features apparent in Fig. 8. The rate of growth in plume ice mass (due to increased plume volume) is slowest early on when the plume grows only vertically and the descending ellipse about the vortices hardly grows at all; increases dra-

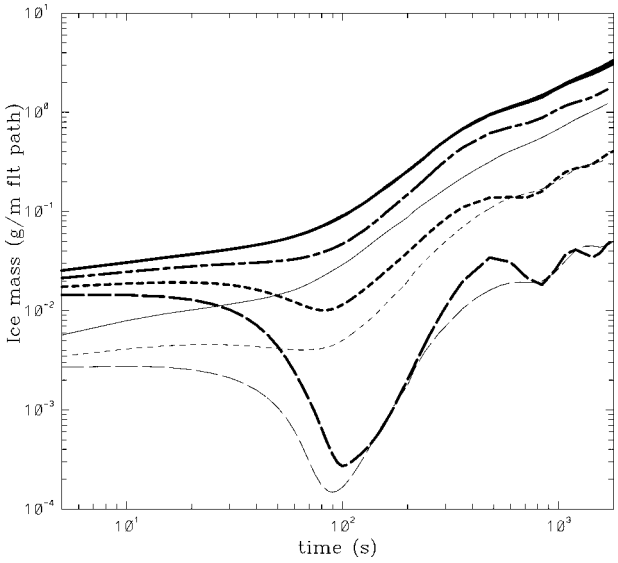

FIG. 8. Total contrail ice mass per length of flight path vs time. Line thickness and dash patterns as in Fig. 7.

matically after linking when the vortex rings distort in all three dimensions and many ice crystals escape from the vortex system; and slows again when the vortex rings dissolve. The Brunt–Väisälä oscillations are just apparent in the variation of the ice mass at late times.

c. Other variations

Figures 10–12 show results analogous to those of Figs. 7–9 for the remaining simulations from Table 2. Consider first the impact of varying the effective ice crystal number emission index. Significantly reducing EI_{iceno} increases the timescale for the plume ice to equilibrate with its local conditions, until it is no longer short compared to the dynamical timescales of the young wake. For the value of $RH_i = 110\%$ chosen in the simulation this gives rise to two competing effects. The larger ice crystals within the vortex system take longer to evaporate completely when the conditions become subsaturated, reducing the fraction that is lost due to adiabatic heating as the vortices fall. Meanwhile the ice mass grows more slowly in the remainder of the plume that is supersaturated. For $EI_{iceno} = 3.7 \times 10^{13}$, both

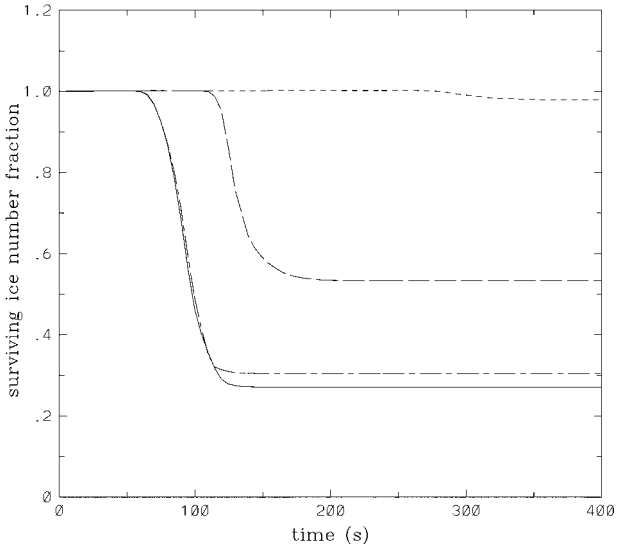

FIG. 10. Fraction of initial ice crystal number surviving vs time for B747 simulations with $RH_i = 110\%$. Here $EI_{iceno} = 10^{15}$ (solid line, simulation A10), $EI_{iceno} = 3.7 \times 10^{13}$ (long dash, simulation A10b), $EI_{iceno} = 10^{12}$ (short dash, simulation A10c), shear = 0.01 s^{-1} (long-short dash, simulation A10d).

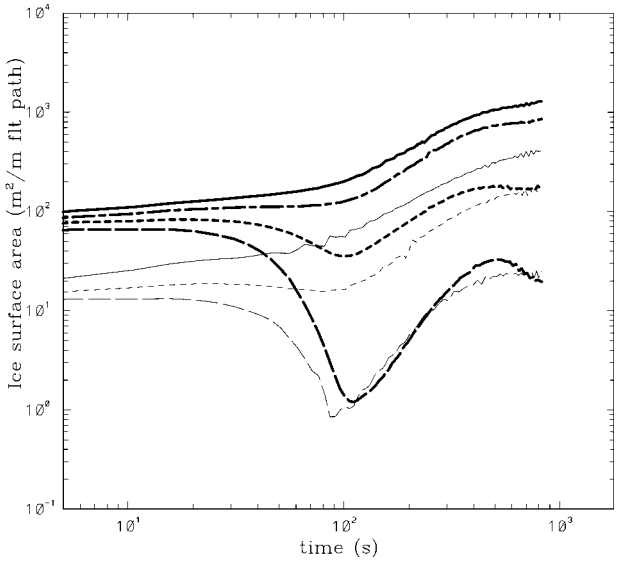

FIG. 9. Total contrail ice surface area per length of flight path vs time. Line thickness and dash patterns as in Fig. 7.

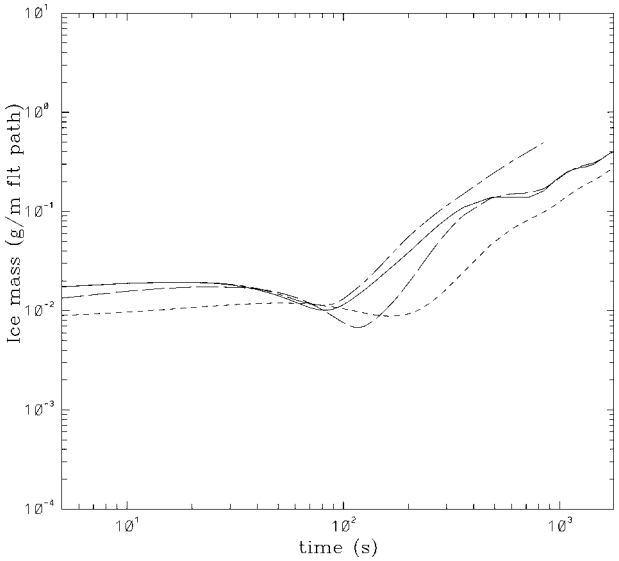

FIG. 11. Total contrail ice mass per length of flight path vs time for B747 simulations with $RH_i = 110\%$. Dash patterns as in Fig. 10.

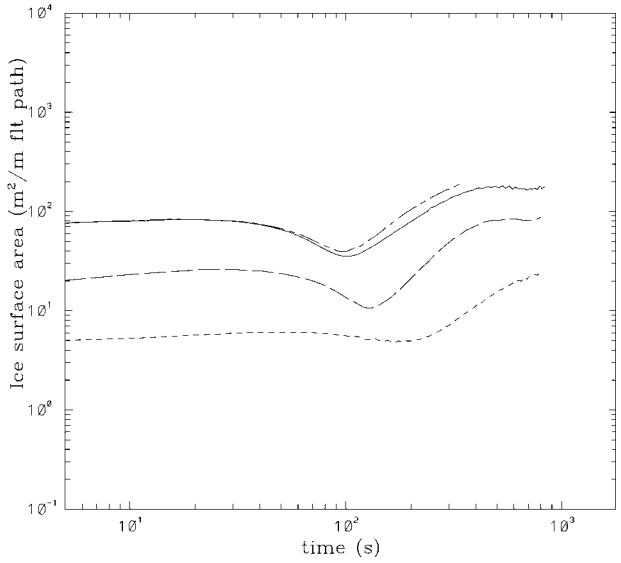

FIG. 12. Total contrail ice surface area per length of flight path vs time for B747 simulations with $RH_i = 110\%$. Dash patterns as in Fig. 10.

effects are modestly important, and from 500 s to 30 min roughly compensate to give the same level of ice mass in the contrail as for the baseline 10^{15} case. (The radiative properties of the contrail would be changed, of course, by the overall change in crystal size and number density.) For $EI_{iceno} = 10^{12}$ the change is dramatic: only a small fraction of the ice crystals evaporate, at the very end of the ring vortex stage, and the overall ice growth lags significantly behind the baseline case. At late enough times this contrail would precipitate away faster as well due to the larger crystal sizes. Our results for this case should be treated as more qualitative than for our other simulations: the sensitivity to the ice microphysics model (and initial ice concentration chosen) increases as the ice number densities are reduced since this increases both the timescale required to achieve ice–vapor equilibrium and the importance of precipitation.

Our treatment here of the effects of wind shear on the contrail development is only cursory. Some is based on results from other simulations (confined to passive tracer dispersion) not presented here. The basic wake decay following through the Crow instability as we have described it remains the principle decay mode in the presence of shear as long as the shear timescale, $1/S$, remains large enough in comparison to the characteristic timescale for the vortex dynamics, t_l. This is the case for both simulations, A30c and A10d, considered here. In the former case, the weak shear has no effect on the vortex dynamics, but does strongly affect the appearance of the contrail at late times, by horizontally smearing it. There is little turbulence or mixing associated with this smearing, however, so that the plume volume and total ice mass remain unchanged (cf. Fig. 8). In simulation A10d the shear is strong enough to noticeably perturb the vortex dynamics. As seen in Fig. 13 the vortex core whose vorticity is aligned counter to the ambient shear is weaker and develops a stronger sinusoidal distortion than its partner. The vortex linking occurs earlier (due to higher ambient turbulent levels) and there is somewhat more detrainment of fluid from the descending vortex system, leading to a slightly higher survival rate for the ice crystals. The most significant

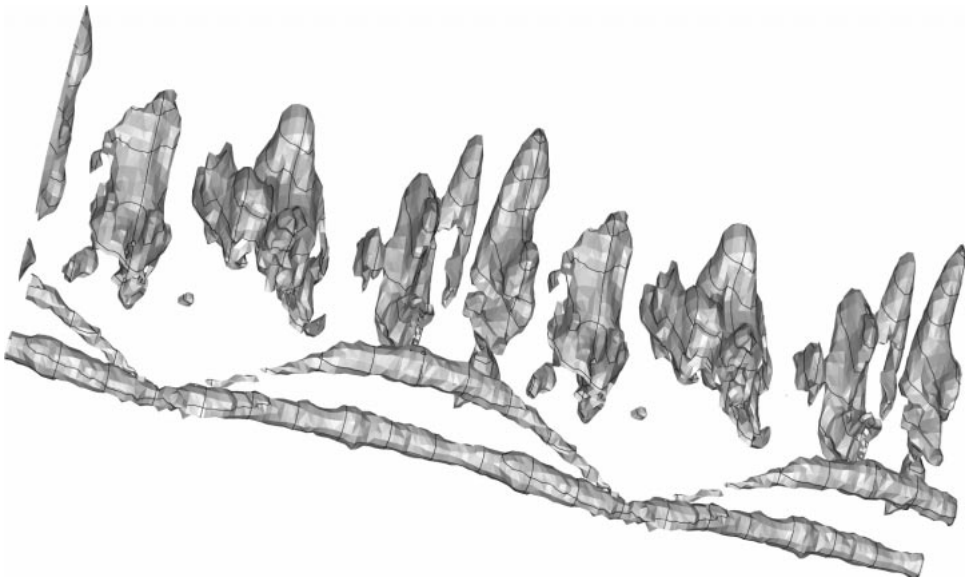

FIG. 13. Three-dimensional isosurface of ice crystal surface area density = 0.005 m^{-1} for a simulated B747 contrail with $RH_i = 110\%$ and shear = 0.01 s^{-1} (simulation A10d) at an age of 90 s. The downstream domain length shown is 600 m.

change is again later in the contrail evolution: during the buoyant plume stage the shear leads to greater mixing and the ice mass accordingly grows at a faster rate.

We conclude this section with a brief qualitative discussion of the effects of some parameters we have not varied in this study: the level of ambient turbulence, stratification, temperature, and pressure. To a limited extent, we have varied the first two of these in other simulations with passive tracer dispersal (not presented here). An increase in the level of ambient turbulence speeds up the onset of vortex linking, increases the degree of downstream inhomogeneity in the exhaust distribution, increases detrainment of exhausts from the descending vortex system, decreases the lifetime of the vortex rings and their total descent distance, and increases mixing in the older contrail. For low to medium ice supersaturations all of these effects tend to increase the contrail ice, either by reducing the fraction of crystals lost to adiabatic heating or by increasing the volume of the plume. For large supersaturations where all the ice crystals survive, the decrease in ring lifetime reduces the vertical extent of the plume, tending to decrease its volume.

In an earlier set of B737 simulations we varied the ambient stratification between 0.001 and 0.01 K m^{-1}. Increasing stratification increases detrainment, decreases vertical plume extent by slowing the vortex descent and by shortening the vortex ring lifetime, and leads to the Brunt–Väisälä oscillation damping out sooner. We found a decrease in vertical plume extent of a factor of two from the increase in lapse rate of an order of magnitude. For large lapse rates one would expect on dimensional grounds a larger effect than this (the vertical extent scaling as $1/N$) but for sufficiently weak lapse rates it is the vortex ring oscillations and diffusion that set the lifetime, independent of the lapse. Whether increased stratification increases or decreases the persistent contrail ice mass will depend on the ambient humidity. For large ambient supersaturation the contrail ice will be reduced because of the decrease in growth of the plume volume. For low to medium supersaturation (particularly for the B747) an increase in stratification can eventually lead to an increase in ice mass by reducing the fraction of ice crystals lost to adiabatic heating. The increased survival rate arises from reducing the total descent and increasing the detrainment during descent.

All of the simulations we have presented in this work were conducted for the same ambient temperature and pressure. At the simplest level of approximation for a persistent contrail we can neglect the contribution of water from the engine exhausts (as it represents only a small fraction of the total ice mass), as well as the perturbation pressure effects, ambient lapse rate, latent heating, departures from ice–vapor equilibrium, and details of the ice microphysics. In equilibrium (which is a good approximation where the ice crystal number densities are sufficiently large), the local ice mass density within the contrail will be given by $\rho q_{si}(\mathrm{RH}_i - 1)$. If we could neglect the adiabatic heating due to vortex descent then the ice mass density within the contrail would be approximately constant in space, varying with T and P (for fixed RH_i) as ρq_{si} does. The evolving shape of the contrail volume would be set by the dispersion of the engine exhausts (via the wake dynamics), independent of T and P. With the adiabatic heating due to vortex descent included, the contrail's spatial distribution depends strongly on RH_i, as we have seen, but is otherwise not strongly dependent on T and P over a reasonable range of cruise conditions. This is because the fractional change in q_{si} in a parcel due to adiabatic descent of a few hundred meters or less is approximately independent of changes in T and P, which are small compared to T and P themselves (in absolute units). In other words, for fixed RH_i significantly above 1, varying T and P scales the ice mass density as ρq_{si} changes but leaves the spatial distribution approximately unchanged. There are corrections to this simple picture that can be important in some limits. For example, for fixed ambient RH_i, the fraction of the contrail ice mass originating from the aircraft engines increases as the ambient q_{si} drops—leading to an increase in the survival rate of the ice crystals for fixed ambient RH_i. And processes scaling with the ice mass, which may become very important in the older persistent wake, particularly latent heating, radiative cooling and precipitation, will increase and affect the wake evolution differently as q_{si} (and hence the total ice mass) increases for fixed RH_i.

5. Summary and comments

In this work we have used large eddy simulations to explore what effects the aircraft wake dynamics may have on persistent contrails. It has been known for a long time that the water emitted from the aircraft engines is responsible for only a tiny fraction of the total ice mass within a large persistent contrail, the bulk originating from the supersaturated ambient air (Knollenberg 1972). The most important effect of the aircraft is to provide ice crystals where they might not otherwise be present, ice nucleation proceeding easily following the formation of droplets in the early water-saturated jet plume. The aircraft wake dynamics affects this process in at least three ways: it largely governs the vertical and horizontal dispersion of the engine exhausts; the low pressure in the vortex cores increases the relative humidity there; and the rapid descent of the vortex system can evaporate some of the ice crystals via adiabatic compression.

In our simulations we have found that the ice crystal number densities generally remain high enough that the ice is near thermodynamic equilibrium within most of the contrail during its evolution. Consequently the ice mass grows proportionally with the plume volume, which in turn is largely determined by vortex dynamics (until ~4 min) and Brunt–Väisälä oscillations (until ~20

min). The loss of ice crystals induced by the vortex descent and adiabatic compression (for low to moderate ice supersaturations) effectively raises the level of supersaturation in the atmosphere required for the production of significant persistent contrails, though by an amount that depends on many factors. The fraction of ice crystals lost through this mechanism depends on a competition between the rate of descent of the vortex system and the rate of mixing between this fluid and the supersaturated ambient fluid. This involves the full 3D wake vortex dynamics, depending on aircraft type as well as on the ambient relative humidity, turbulence level, shear, and stratification. Consequently, the simple assumption often made that the ice mass in a contrail for given ambient conditions is proportional to fuel usage is not true in general; a B737, for example, can give rise to as significant a persistent contrail as a B747 under conditions with moderate ambient ice supersaturations.

In concentrating on the effects of the aircraft wake dynamics on contrail development, we have considered neither the initial contrail formation nor its long-term fate or impact. Addressing whether or when the radiative properties of contrails lead to significant cooling or warming, or the precipitation of ice crystals leads to important redistribution of atmospheric moisture, generally requires following the contrail's evolution over longer time periods than we have considered here. To extend the simulations here to address such issues would require an improved ice microphysics model to better treat the radiative properties and precipitation as these become important effects. A better treatment of the ambient atmospheric turbulence would be desirable as well since after the decay of the wake dynamics it will largely govern the contrail spread. The turbulence in the preferred flight corridors is largely intermittent, generated by occasional wave–wave interactions, for example, and so is challenging to simulate in its own right.

We have considered only a very limited range of atmospheric conditions and flight scenarios, as well. Other shear and turbulence conditions or aircraft platforms could be profitably explored. More complex background temperature and humidity profiles could lead to other interesting effects, for example, wake dynamics triggering the release of a conditional instability in the profile (cf. Gierens and Jensen 1998).

Having identified some significant effects of the aircraft wake dynamics on the long-term development of persistent contrails, it is natural to speculate on whether there is any obvious strategy for minimizing their occurrence or extent, short of restricting flight traffic to drier air masses. Such strategies might focus on minimizing either contrail dispersion or surviving ice crystal number. Unfortunately, these goals often conflict, and a strategy that might be beneficial for one set of atmospheric conditions could easily prove to be detrimental for some others. Sussmann and Gierens (1999) suggest using heavy aircraft and minimizing detrainment, for example, by shifting the engine position closer to the wing tips so that the exhausts are all captured within the vortex cores. For the low humidity case that they consider, or case A2 (and possibly A10) here, this would probably work admirably, with the contrail ice effectively all evaporated by the adiabatic heating. For high supersaturations, such as case A30, however, where the ice crystals will survive the vortex descent, this is a good recipe for maximizing the mixing of the ice crystals throughout the full plume volume. Concentrating the exhausts in the cores also concentrates the water originating from the engines and maximizes the impact of the dynamic pressure drop in the core. Consequently, there is probably a window of atmospheric conditions for which the ice crystals within the cores would survive descent while if they had been less tightly bound, in the ellipse of fluid descending around the vortices, they would not have.

The reverse strategy of trying to get all of the exhausts to escape the descending vortex system suffers from the opposite problem. It serves to minimize the volume occupied by the ice crystals but eliminates the possibility of crystal loss through adiabatic descent, thus it helps for large supersaturations and hinders for smaller. Similarly, reducing EI_{iceno} (perhaps by burning different fuels) would generally prove beneficial in reducing contrails as one would expect, but might under some conditions ensure the survival of ice crystals throughout the full wake plume volume where adiabatic heating might otherwise have restricted the contrail to the upper portion of the wake. Attempts to minimize the contrail by changing the Crow instability dynamics (e.g., by changing the vortex spacing) suffer from the same compromise: speeding up or increasing the vertical descent to evaporate descending ice crystals serves only to increase the vertical mixing of the plume if the ambient supersaturation is high enough that the crystals survive anyway.

It is not even clear if a smaller number of heavy transports is always better than a larger number of light ones. Given the larger circulations and vortex fall times for the heavier aircraft, their vortex decay is less affected by a given level of wind shear. For some levels of shear the vertical spread of the light aircraft wake due to the vortex dynamics might be effectively suppressed while that for the heavier one is not.

Acknowledgments. This research was supported by NASA's Atmospheric Effects of Aviation Project, Grant NAG-1-2096, with W. L. Grose as technical monitor.

REFERENCES

Anderson, B., W. R. Cofer, D. R. Bagwell, J. W. Barrick, and C. H. Hudgins, 1998: Airborne observations of aircraft aerosol emissions. I: Total nonvolatile particle emission indices. *Geophys. Res. Lett.*, **25,** 1689–1692.

Bliss, D. B., 1982: Effect of unsteady forcing on the sinusoidal instability of vortex wakes. *J. Aircr.*, **19,** 713–721.

Böhm, H. P., 1989: A general equation for the terminal fall speed of solid hydrometeors. *J. Atmos. Sci.,* **46,** 2419–2427.

Brown, R. C., R. C. Miake-Lye, M. R. Anderson, and C. E. Kolb, 1997: Aircraft sulfur emissions and the formation of visible contrails. *Geophys. Res. Lett.,* **24,** 385–388.

Chlond, A., 1998: Large-eddy simulations of contrails. *J. Atmos. Sci.,* **55,** 796–819.

Corjon, A., and T. Poinsot, 1997: Behavior of wake vortices near ground. *AIAA J.,* **35,** 849–855.

Crow, S. C., 1970: Stability theory for a pair of trailing vortices. *AIAA J.,* **8,** 2172–2179.

Ebert, E. E., and J. A. Curry, 1992: A parameterization of ice cloud optical properties for climate models. *J. Geophys. Res.,* **97** (D4), 3831–3836.

Farnell, L., 1980: Solution of Poisson equations on a nonuniform grid. *J. Comput. Phys.,* **35,** 408–425.

Gerz, T., and T. Ehret, 1996: Wake dynamics and exhaust distribution behind cruising aircraft. *Proc. AGARD Symp.,* Trondheim, Norway, CP-584, 35.1–35.12.

——, T. Dürbeck, and P. Konopka, 1998: Transport and effective diffusion of aircraft emissions. *J. Geophys. Res.,* **103,** 25 905–25 913.

Gierens, K., and E. Jensen, 1998: A numerical study of the contrail-to-cirrus transition. *Geophys. Res. Lett.,* **25,** 4341–4344.

Gierens, K. M., 1996: Numerical simulations of persistent contrails. *J. Atmos. Sci.,* **53,** 3333–3348.

——, and J. Ström, 1998: A numerical study of aircraft wake induced ice cloud formation. *J. Atmos. Sci.,* **55,** 3253–3263.

Hall, W. D., and H. R. Pruppacher, 1976: The survival of ice particles falling from cirrus clouds in subsaturated air. *J. Atmos. Sci.,* **33,** 1995–2006.

Heymsfield, A. J., L. M. Milosevich, C. Twohy, G. W. Sachse, and S. Oltmans, 1998: Upper-tropospheric relative humidity observations and implications for cirrus ice nucleation. *Geophys. Res. Lett.,* **25,** 1343–1346.

Jensen, E. J., A. S. Ackerman, D. E. Stevens, O. B. Toon, and P. Minnis, 1998: Spreading and growth of contrails in a sheared environment. *J. Geophys. Res.,* **103,** 31 557–31 567.

Kärcher, B., T. Peter, U. M. Biermann, and U. Schumann, 1996: The initial composition of jet condensation trails. *J. Atmos. Sci.,* **53,** 3066–3083.

——, R. Busen, A. Petzold, F. Schröder, U. Schumann, and E. Jensen, 1998: Physicochemistry of aircraft-generated liquid aerosols, soot, and ice particles. Part 2. Comparison with observations and sensitivity studies. *J. Geophys. Res.,* **103,** 17 129–17 147.

Khvorostyanov, V., and K. Sassen, 1998: Cloud model simulation of a contrail case study: Surface cooling against upper tropospheric warming. *Geophys. Res. Lett.,* **25,** 2145–2148.

Knollenberg, R. G., 1972: Measurement of the growth of the ice budget in a persisting contrail. *J. Atmos. Sci.,* **29,** 1367–1374.

Koenig, L. R., 1971: Numerical modeling of ice deposition. *J. Atmos. Sci.,* **28,** 226–237.

Lewellen, D. C., and W. S. Lewellen, 1996: Large-eddy simulations of the vortex-pair breakup in aircraft wakes. *AIAA J.,* **34,** 2337–2345.

——, ——, L. R. Poole, R. J. DeCoursey, G. M. Hansen, and C. A. Hostetler, 1998: Large-eddy simulations and lidar measurements of vortex-pair breakup in aircraft wakes. *AIAA J.,* **36,** 1439–1445.

——, ——, and J. Xia, 2000: The influence of a local swirl ratio on tornado intensification near the surface. *J. Atmos. Sci.,* **57,** 527–544.

Minnis, P., D. F. Young, L. Ngyuen, D. P. Garber, W. L. Smith Jr., and R. Palikonda, 1998: Transformation of contrails into cirrus during SUCCESS. *Geophys. Res. Lett.,* **25,** 1157–1160.

Penner, J. E., D. H. Lister, D. J. Griggs, D. J. Dokken, and M. McFarland, Eds., 1999: *Aviation and the Global Atmosphere: Special Report of the Intergovernmental Panel on Climate Change.* Cambridge University Press, 373 pp.

Quackenbush, T. R., M. E. Teske, and A. J. Bilanin, 1996: Dynamics of exhaust plume entrainment in aircraft vortex wakes. AIAA Paper 96-0747, 15 pp. [Available online at www.aiaa.org.]

Robins, R. E., and D. P. Delisi, 1997: Numerical simulation of three-dimensional trailing vortex evolution. *AIAA J.,* **35,** 1552–1555.

Rogers, R. R., 1976: *A Short Course in Cloud Physics.* Pergamon Press, 227 pp.

Schaefer, V. J., and J. A. Day, 1981: *The Peterson Field Guide to the Atmosphere.* Houghton Mifflin, 359 pp.

Schröder, F., and Coauthors, 2000: On the transition of contrails into cirrus clouds. *J. Atmos. Sci.,* **57,** 464–480.

Schumann, U., 1996: On conditions for contrail formation from aircraft exhausts. *Meteor. Z.,* **5,** 4–23.

Scorer, R. S., and L. J. Davenport, 1970: Contrails and aircraft downwash. *J. Fluid Mech.,* **43,** 451–464.

Spalart, P. R., 1998: Airplane trailing vortices. *Annu. Rev. Fluid Mech.,* **30,** 107–138.

——, and A. A. Wray, 1996: Initiation of the Crow instability by atmospheric turbulence. *Proc. AGARD Symp.,* Trondheim, Norway, CP-584, 18.1–18.8.

Stephens, G. L., 1983: The influence of radiative transfer on the mass and heat budgets of ice crystals falling in the atmosphere. *J. Atmos. Sci.,* **40,** 1729–1739.

Sussmann, R., and K. M. Gierens, 1999: Lidar and numerical studies on the different evolution of vortex pair and secondary wake in young contrails. *J. Geophys. Res.,* **104,** 2131–2142.